THE JOURNAL OF PHYSICAL CHEMISTRY C

Article

Cite This: J. Phys. Chem. C 2019, 123, 29580−29588

pubs.acs.org/JPCC

Barrierless Heptazine-Driven Excited State Proton-Coupled Electron Transfer: Implications for Controlling Photochemistry of Carbon Nitrides and Aza-Arenes

Emily J. Rabe,[†] Kathryn L. Corp,[†] Xiang Huang,[∥] Johannes Ehrmaier,[∥] Ryan G. Flores,[†] Sabrina L. Estes,[†] Andrzej L. Sobolewski,[⊥] Wolfgang Domcke,[∥] and Cody W. Schlenker*[,†,‡,§]

[†]Department of Chemistry, University of Washington, Seattle, Washington 98195, United States

[‡]Molecular Engineering & Sciences Institute, University of Washington, Seattle, Washington 98195-1652, United States

[§]Clean Energy Institute, University of Washington, Seattle, Washington 98195-1653, United States

[∥]Department of Chemistry, Technical University of Munich, D-85747 Garching, Germany

[⊥]Institute of Physics, Polish Academy of Sciences, PL-02668 Warsaw, Poland

Supporting Information

ABSTRACT: To inform prospective design rules for controlling aza-arene photochemistry, we studied hydrogen-bonded complexes of 2,5,8-tris(4-methoxyphenyl)-1,3,4,6,7,9,9b-heptaazaphenalene (TAHz), a molecular photocatalyst chemically related to graphitic carbon nitride, with a variety of phenol derivatives. We have focused on excited state proton-coupled electron transfer (ES-PCET) reactions of heptazines because the excited state properties governing this process remain conceptually opaque compared to proton reduction reactions for these materials. We used ground-state absorption, time-resolved photoluminescence, and ab initio quantum chemical calculations to analyze TAHz reactivity toward a series of six para-substituted phenol derivatives. We determined association constants (K_A), excited-state quenching rate constants (k_Q), kinetic isotope effects, and transition-state barriers ($\Delta E^{\ddagger}$). From this data, we provide a generalizable picture of hydrogen bond formation and excited state reactivity of heptazine-based materials with hydrogen-atom donating solvents. These results provide important insights into strategies to tune charge transfer state energies and increase ES-PCET rates.

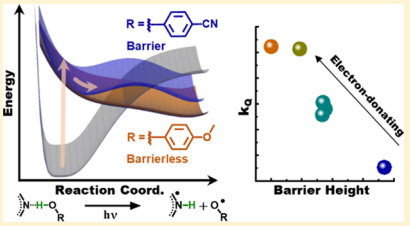

1. INTRODUCTION

Concerted motion of protons and electrons is critical for a variety of chemical transformations relevant for applications spanning energy storage[1,2] to municipal wastewater treatment.[3,4] Recently, there has been mounting world-wide interest in deploying molecular and polymeric organic constructs as photoredox catalysts to drive these transformations using photons.[5−7] In order to utilize solar energy in such processes, it is desirable to understand what molecular properties control the efficiency of intermolecular excited state proton-coupled electron transfer (ES-PCET) reactions. The majority of intermolecular ES-PCET literature to date focuses on metal-containing complexes,[8−11] with fewer examples of all-organic chromophores,[12−14] despite their photophysical properties being extensively studied over the past century.[5,6,15−17] Precious metal-containing catalysts have become promising candidates, in part, because of their long-lived excited state lifetimes ranging from hundreds of nanoseconds to microseconds.[18] However, identifying earth-abundant alternatives continues to be a compelling challenge to overcome. We have elected to examine all-organic materials with long excited state lifetimes and good photostability. Recently, the nitrogen-rich heptazine (Hz) unit has garnered increased attention for applications in photocatalytic hydrogen production.[7,19−21] The mechanism of molecular Hz-driven ES-PCET has been studied computationally,[22−24] and our group reported the first experimental evidence for this process resulting in neutral radical species.[25] This Hz-based chromophore exhibits a singlet lifetime of 296.9 ± 0.4 ns, the same order of magnitude as $[Ru(bpy)_3]^{2+}$, a compound which is ubiquitous in the study of photochemical transformations.[18,26] Interestingly, this roughly 300 ns lifetime is significantly longer than first row transition-metal complexes[27] as well as traditional strongly absorbing organic chromophores, which typically have lifetimes of no more than tens of nanoseconds.[28] Additionally, we previously reported computational and experimental evidence that Hz derivatives can exhibit an extremely unusual inversion of the energies of their lowest singlet and triplet excited states.[29] This peculiar violation of Hund's multiplicity rule stands in contrast to virtually all other classes of known organic compounds. With the lowest-lying excited state being a singlet rather than a triplet, the sensitization of singlet oxygen appears to become an inaccessible decay pathway for the lowest energy excited state

Received: September 17, 2019
Revised: November 17, 2019
Published: November 18, 2019

DOI: 10.1021/acs.jpcc.9b08842
J. Phys. Chem. C 2019, 123, 29580−29588

of many Hz-based chromophores. Those results imply that Hz molecules should enjoy unique photostability in the presence of oxygen while maintaining a long-lived excited state (see Section SII).

Herein, we provide further mechanistic insights into intermolecular ES-PCET using 2,5,8-tris(4-methoxyphenyl)-1,3,4,6,7,9,9b-heptaazaphenalene (TAHz) with a series of phenol (PhOH) derivatives as proton and electron donors, shown in Figure 1. By altering the functional group on PhOH, we monitor the effect of redox potential and hydrogen bonding on the resulting photochemical reaction.[30−34] In particular, we consider the energy of the intermolecular charge transfer (CT) states that form in these complexes and the corresponding excited state reaction barrier heights. For each phenol derivative, we determine a quenching rate constant (k_Q) of photoexcited TAHz, an association constant (K_A), and a kinetic isotope effect (KIE) of excited state deactivation with R−PhOH versus R−PhOD. As the electron-donating strength of the para-substituent, R, on R−PhOH is increased, we observe an increase in the quenching rate constant accompanied by a decrease in KIE. Using ab initio quantum chemical calculations to examine the energy landscape for the interaction of the Hz core with the same series of PhOHs, we observe the same trend, wherein the transition-state barrier for the photoinduced reaction decreases until the reaction becomes completely barrierless for the most electron-donating PhOH, OCH_3−PhOH. Using time-resolved photoluminescence (TR-PL) measurements and global analysis, we can separately monitor hydrogen-bonded and free TAHz emission. Correspondingly, we observe no evidence for emission from hydrogen-bonded complexes in the case of OCH_3−PhOH, consistent with barrierless excited state reactivity. This photochemical reactivity information provides new insights that synthetic chemists and materials scientists can deploy to outline new molecular design strategies targeting Hz-based photocatalysis.

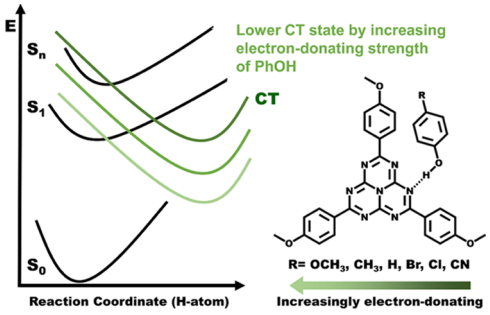

Figure 1. Schematic depiction of the proposed excited state landscape along the H-atom transfer coordinate from phenol (PhOH) to TAHz. As proposed previously, there exists a CT state in which an electron moves from the oxygen atom of PhOH to the heptazine core and can drive proton motion. Previous studies with TAHz and water suggested the CT state was accessible from higher-lying states. We hypothesized that the energy curve of the CT state could be stabilized by adding electron-donating groups on the H-atom donor. In this study, we do this by using the series of R−PhOH derivatives depicted above.

2. RESULTS AND DISCUSSION

2.1. Association Constants for Hydrogen Bonding.

We observe evidence for hydrogen bonding by comparing the ground-state absorption spectra of TAHz with and without

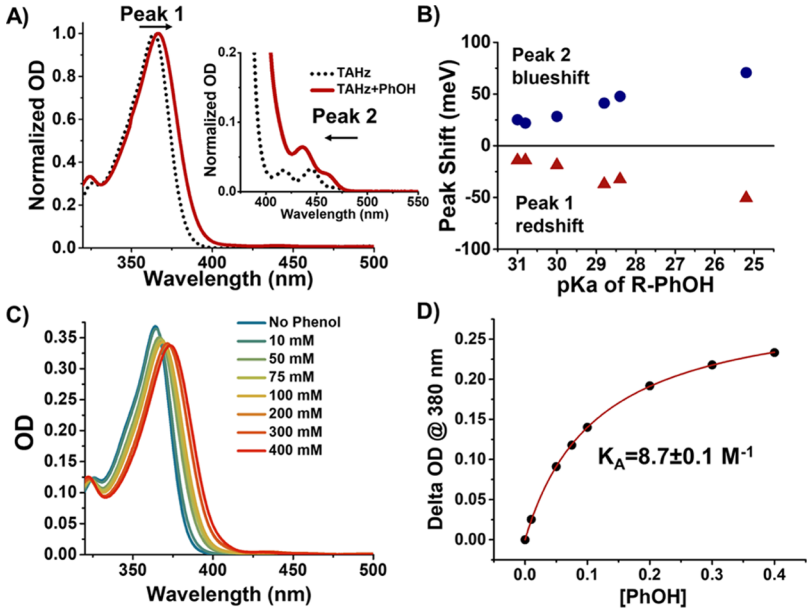

Figure 2. (A) Addition of phenol (PhOH) changes the ground-state absorption of TAHz in toluene, suggesting hydrogen bonding. A distinct redshift of the main absorption can be seen from TAHz in toluene without PhOH present (black dotted line) upon the addition of 100 mM PhOH (solid red line). The weakly allowed transitions at lower energies, on the other hand, exhibit a blueshift upon addition of PhOH, shown in the inset. (B) Peak shifts of TAHz absorption with 100 mM of R−PhOH as a function of the PhOH's pK_a [in dimethyl sulfoxide (DMSO)] shows a largely linear trend. This suggests that different PhOHs have different hydrogen bonding strengths with TAHz. (C) Absorption spectra of TAHz with different PhOH concentrations show change toward the TAHz−PhOH complex absorption. (D) Change in absorption intensity (ΔOD) at 380 nm as a function of PhOH concentration shows the TAHz absorption spectrum asymptotically approaching that of the all-hydrogen-bonded complex. Fitting the data to eq 1, we determined K_A for TAHz and PhOH to be 8.7 ± 0.1 M^{-1}.

DOI: 10.1021/acs.jpcc.9b08842
J. Phys. Chem. C 2019, 123, 29580−29588

Table 1. Comparison of Key Parameters Determining Hydrogen Bonding and ES-PCET in Complexes of TAHz or Hz with Phenol (PhOH) Derivatives

R	E_0 ($RPhOH^+/RPhOH$)[a]	pK_a PhOH[b]	k_Q ($\times 10^9$ s^{-1}) TCSPC	k_Q ($\times 10^9$ s^{-1}) PLQY	K_A (M^{-1})	S_1 KIE[c]	R_{NH} (Å)[d]	$\Delta E^{\ddagger}$ (eV)[d]
CN	2.03	13.2	0.556 ± 0.05	0.53 ± 0.02	58 ± 3	1.9 ± 0.1	1.904	0.369
Cl	1.88	16.75	2.78 ± 0.03	2.785 ± 0.007	17.2 ± 0.3	1.36 ± 0.04	1.924	0.169
Br	1.86	16.36	2.73 ± 0.03	3.053 ± 0.009	19.1 ± 0.7	1.36 ± 0.05	1.923	0.177
H	1.88	18.0	2.21 ± 0.02	2.579 ± 0.004	8.7 ± 0.1	1.5 ± 0.1	1.937	0.167
CH_3	1.79	18.9	4.21 ± 0.02	5.124 ± 0.007	8.9 ± 0.2	1.19 ± 0.04	1.940	0.093
OCH_3	1.68	19.1	4.26 ± 0.03	5.218 ± 0.008	8.9 ± 0.4	1.06 ± 0.02	1.943	

[a]Versus SHE in ACN (±0.1 V).[33,39] [b]In DMSO.[34] [c]All R−PhOH concentrations 50 mM. [d]From ab initio calculations, see Section 2.4.

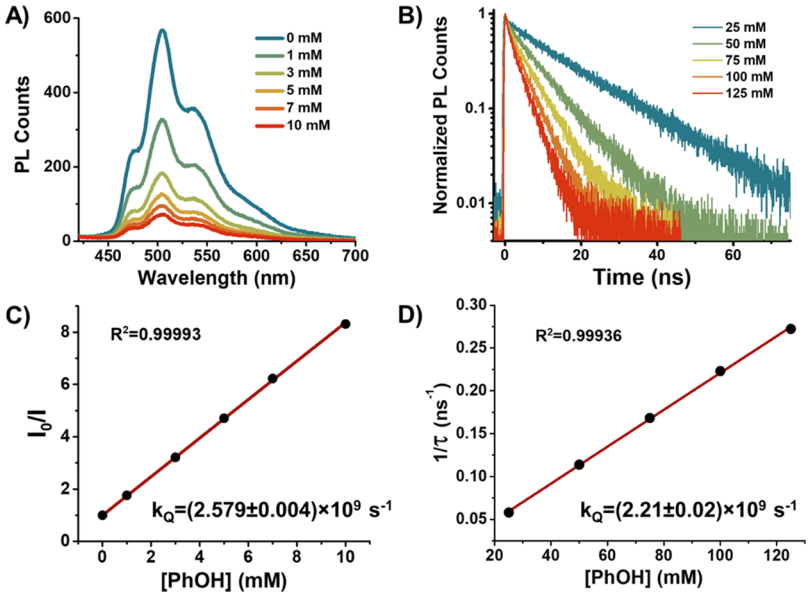

Figure 3. (A) PL intensity quenching of TAHz shows significant static quenching with increasing concentrations of phenol (PhOH). (B) PL lifetimes of TAHz with increasing concentrations of PhOH show dynamic quenching. Stern−Volmer analysis yields quenching constants, k_Q, for (C) PL intensity quenching and (D) PL lifetime, fit after 5 ns.

PhOH present, as shown in Figure 2A. Upon hydrogen bonding, we see a redshift in the bright $\pi\pi^*$ transition, labeled "peak 1." At lower energies, we observe a blueshift of the weakly allowed transitions with $n\pi^*$ character, labeled "peak 2." Figure 2B shows the magnitude of the peak shift as a function of the pK_a of the PhOH derivative. PhOHs with electron-donating substituents, such as CH_3−PhOH and OCH_3−PhOH, show only small shifts, whereas CN−PhOH displays a significantly larger shift at 50 mM PhOH concentrations. This suggests that the hydrogen bonding strength is not equal across the series of PhOH derivatives. The calculations (see Section SVIII) show the length of the hydrogen bond between the OH group of PhOH and the acceptor N-atom of Hz (R_{NH}) is 1.937 Å in the Hz−PhOH complex. R_{NH} increases to 1.943 Å for the strongest electron donating substituent (OCH_3) and decreases to 1.904 Å for the strongest electron withdrawing substituent (CN), see Table 1. As is well known, the length of the hydrogen bond is a proxy for the strength (binding energy) of the latter. In order to quantify these differences from the experimental side, we determined the association constant between TAHz and each of the six PhOH derivatives. We employed the method previously used by the Hammarström group to fit the saturation behavior of the changing ground-state absorption as a function of PhOH concentration.[35,36] Figure 2C shows the change in absorption spectra for TAHz with increasing PhOH concentrations. Figure 2D plots the change in optical density as a function of PhOH concentration, showing a clear saturation behavior. Fitting this data to eq 1 allows us to extract a K_A value for TAHz−PhOH in the ground state.

$$\frac{\Delta A}{l} = \Delta\varepsilon_{380}\left(\frac{[\mathrm{TAHz}]_0 + [\mathrm{PhOH}]_0 + K_A^{-1}}{2}\right) \pm \sqrt{\left(\frac{[\mathrm{TAHz}]_0 + [\mathrm{PhOH}]_0 + K_A^{-1}}{2}\right)^2 - [\mathrm{TAHz}]_0[\mathrm{PhOH}]_0} \quad (1)$$

Here ΔA is the change in absorption at a given wavelength, l is the path length of the cuvette, $\Delta\varepsilon_{380}$ is the difference in molar absorptivity at 380 nm between the bound TAHz−PhOH complex and free TAHz chromophore; $[\mathrm{TAHz}]_0$ and $[\mathrm{PhOH}]_0$ are the initial concentrations of TAHz and PhOH, respectively.

Using eq 1, we have estimated the K_A values for the six PhOH derivatives with TAHz in Table 1 (see Section SIII for fits). As expected, we see an increased K_A for PhOHs with electron-withdrawing substituents with the largest being for CN−PhOH. Notably, there is a very small difference between the K_A values for PhOH, CH_3−PhOH, and OCH_3−PhOH, despite there being a significant difference between the oxidation potentials of these PhOHs. The computed ground-state hydrogen bond lengths follow the same trend.

DOI: 10.1021/acs.jpcc.9b08842
J. Phys. Chem. C 2019, 123, 29580−29588

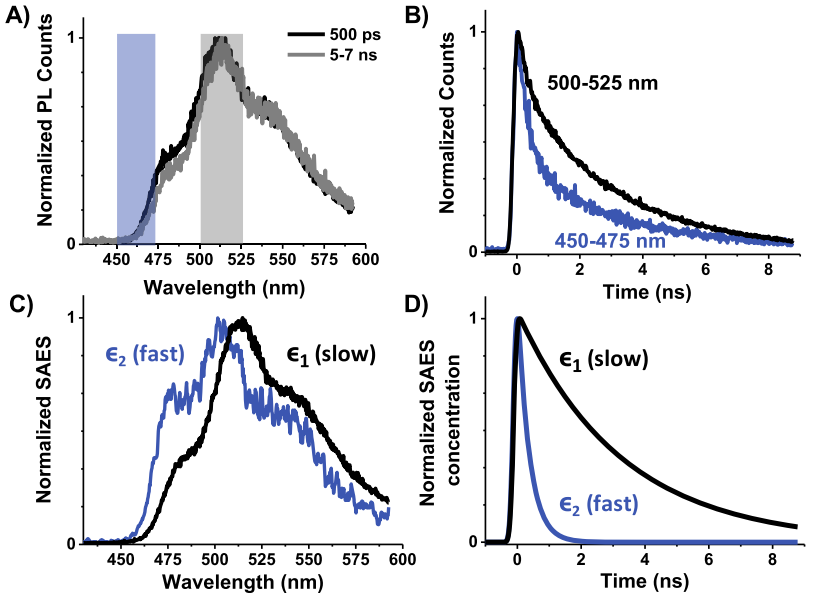

Figure 4. (A) TR-PL measurements of 50 μM TAHz with 100 mM phenol. Spectral traces averaged over the first 500 ps (black) and 5−7 ns (gray) show a small spectral change in the high-energy region. (B) Kinetic decay traces averaged from 450 to 475 nm (blue) and 500 to 525 nm (black) suggest at least two kinetically distinct luminescent species. (C,D) Global target analysis of the TR-PL data shows two SAES. Emission attributed to the S_1 state, labeled ϵ_1 (black), is the emission shape seen in steady-state measurements and has a lifetime of 3.23 ns. The second SAES, labeled ϵ_2 (blue), is seen at higher energies and decays notably faster than ϵ_1 with a lifetime of 0.36 ns.

To determine how these ground-state electrochemical and hydrogen-bonding properties affect the photochemical reactivity and excited state barrier height, we turn to PL quenching and ab initio computational studies.

2.2. Quenching Constants for PhOH Derivatives. To monitor the quenching rate of the TAHz S_1 state with varying PhOH derivatives, we performed Stern−Volmer quenching analysis using both PL intensity and lifetime quenching data as shown in Figure 3A,B, respectively. Table 1 holds all of the k_Q values for the six different PhOHs (see Section SIV) and calculated KIE values for the S_1 lifetime with R−PhOH/D. As expected, increasingly anodic oxidation potentials of the R−PhOH lead to smaller k_Q values, suggesting that a kinetic barrier has been introduced along the photochemical reaction pathway. This is confirmed by the increasing KIE values with decreasing k_Q, suggesting proton motion must couple to electron motion for the reaction to proceed, perhaps by a tunneling mechanism. In the cases of low KIE values and high k_Q constants, it is plausible that the mechanism of fluorescence quenching can be attributed to pure electron transfer (ET), as has been discussed previously.[33,37] However, when we monitored TAHz fluorescence quenching in the presence of the pure electron donor 1,4-dimethoxybenzene, with an oxidation potential similar to OCH_3−PhOH but without the capacity to transfer a proton, we observed only moderate quenching that was roughly seven times slower than OCH_3−PhOH (see Section SV for further discussion).[38] This suggests that, while ET to TAHz is observable, the fast quenching rates we observe with phenols do not appear to be consistent with a purely donor−acceptor ET process alone.

The experimentally determined k_Q values from the two methods (intensity and lifetime) are close for PhOH, but the intensity quenching shows a slightly greater rate constant. We attribute this to the fact that intensity analysis can reflect both static and dynamic quenching, whereas lifetime analysis only captures the rate of dynamic quenching. We note that for PhOH derivatives with low K_A values and low oxidation potentials, we see a greater difference between the k_Q values that we obtain from lifetime measurements compared with intensity measurements. One explanation could be, in this case, that complex formation is the rate-determining step as opposed to ES-PCET. Whereas in the case of CN−PhOH, K_A is large but the driving force for ET is low, so the rate of ES-PCET is rate-determining. In this case, the intensity and lifetime quenching are the same because both report on the rate of ES-PCET.

It is worth noting that we observed a two-component PL lifetime in the presence of PhOH, in contrast to the monoexponential decay of TAHz in neat toluene. We attributed the fast decay to the emission of hydrogen-bonded complexes, as has been observed for coumarin complexes previously.[30] We determined the lifetime k_Q values using the long component of the PL lifetime, see Section SIV for further discussion, and therefore, we regard this value as a reporter on diffusional quenching.

2.3. Time-Resolved PL. Using TR-PL spectra in tandem with global analysis, we analyzed the nature of the fast PL decay component mentioned above. Figure 4A shows the PL spectral traces of TAHz in a 100 mM PhOH solution at early (500 ps) and late (5−7 ns) times. Though the spectral difference is small, the increased intensity near 475 nm at early times does not appear for TAHz in neat toluene (Figure S15). Figure 4B clearly shows different decay rates in the spectral range 450−475 nm in contrast to 500−525 nm, indicating that at least two separate luminescent species are present.

To kinetically resolve these overlapping emission features, we apply global analysis. We model total PL intensity $\Theta(t,\lambda)$ at time t and wavelength λ as a sum of concentration-weighted spectral components such that $\Theta(t,\lambda) = \Sigma c_i(t)\sigma_i(\lambda)$, where $c_i(t)$ and $\sigma_i(\lambda)$, respectively, correspond to the time-dependent concentration and wavelength-dependent species-associated emission spectra (SAES) of the ith emissive species.[40] Global

DOI: 10.1021/acs.jpcc.9b08842
J. Phys. Chem. C 2019, 123, 29580−29588

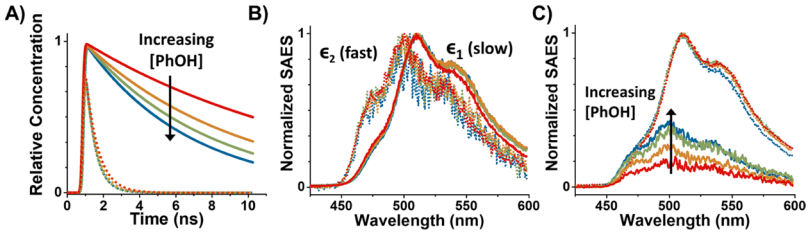

Figure 5. Phenol (PhOH) concentration-dependent TR-PL suggesting that the high energy emission is from a hydrogen-bonded complex. (A) Kinetic decay rates of bonded TAHz S_1 (solid) hydrogen-bonded TAHz–PhOH (dotted) with different PhOH concentrations: 25 mM (red), 50 mM (orange), 75 mM (green), and 100 mM (blue). (B) Normalized SAES reveal that the spectral shape does not appreciably depend on phenol concentration. (C) High-energy emission grows with increasing [PhOH] relative to low-energy emission.

analysis yields two kinetically resolvable emission features as shown in Figure 4C. The spectral trace at higher energies decays at a significantly faster rate, on the order of hundreds of picoseconds. We attribute this emission spectrum to that of a hydrogen-bonded TAHz–PhOH complex. The blueshift in emission corresponds to the blueshift of the low-lying and weakly-allowed transitions that appear in the absorption spectra in Figure 2A. Considering the nπ^* character of these low energy transitions, we would expect to see a blueshift for the emission of this state. It is interesting to note that the vibronic peak spacing is similar for both the fast and slow components of roughly 1200 cm^{-1}, which is commensurate with a heptazine ring-breathing mode.

To probe whether this state is associated with hydrogen bonding between TAHz and PhOH, we monitor the relative amplitude of the emission signal for this high-energy species as a function of PhOH concentration. While Figure 5B shows that the spectral shape does not change for either species, Figure 5C reveals that the relative intensity of the high energy features increases with increasing concentrations of PhOH. This intensity/concentration correlation strongly suggests that the high energy emission results from a hydrogen-bonded TAHz–PhOH complex. This distinction between hydrogen-bonded and free TAHz emission allows us to monitor the two populations separately for the different PhOH derivatives. We observe kinetically resolved high energy emission spectra for all of the phenol derivatives that we studied, with the exception of OCH_3–PhOH, Figure S22, for which this emission feature is absent on our experimental timescale (Supporting Information Section SVI). We attribute this absence to barrierless reactivity from the S_1 state (vide infra). Such barrierless reactivity for OCH_3–PhOH would be consistent with this derivative possessing the lowest anodic oxidation potential in this series and exhibiting no significant KIE. In the photoexcited TAHz and OCH_3–PhOH complex, the rate of reaction far outcompetes the rate of fluorescence. Therefore, the only emission we observe is from unbound TAHz chromophores. The quenching rate of this free TAHz then becomes diffusion limited for the chromophore and OCH_3–PhOH in the solution.

2.4. Computational Studies of Structures and Potential Energy Surfaces of Hz–PhOH Complexes. To assess the role of the excited state reaction barrier in controlling the photochemical reactivity of hydrogen-bonded heptazine–phenol complexes, we turned to ab initio quantum chemical calculations. The ground-state equilibrium geometries of the hydrogen-bonded complexes of Hz with PhOH and derivatives thereof were determined with the second-order Møller–Plesset (MP2) method. Vertical electronic excitation energies and excited state potential energy surfaces were computed with the second-order algebraic diagrammatic construction [ADC(2)] method.[41] ADC(2) is a wave-function-based single-reference propagator method which provides, in contrast to time-dependent density functional theory with various functionals, an accurate and balanced description of locally excited (LE) states and CT states, which is essential for the determination of reliable ab initio potential energy surfaces for ES-PCET reactions. The complex of TAHz with PhOH is too big for wave-function-based excited state ab initio calculations. Therefore, all ab initio calculations were performed for complexes of the Hz core of TAHz with PhOH and its derivatives. More details on the ab initio computational methods are given in Section SVIII of the Supporting Information.

The most relevant nuclear coordinates for PCET processes are the H-atom transfer coordinates (chosen here as the OH bond length R_{OH} of the hydrogen-bonded PhOH molecule) and the distance R_{ON} between the oxygen atom of PhOH and the H-atom accepting nitrogen atom of Hz (Figure 6). For fixed R_{OH} and R_{ON}, the energy of the lowest excited singlet state was minimized with respect to all other nuclear coordinates of the complex. This procedure yields a two-dimensional (2D) relaxed potential energy surface for the

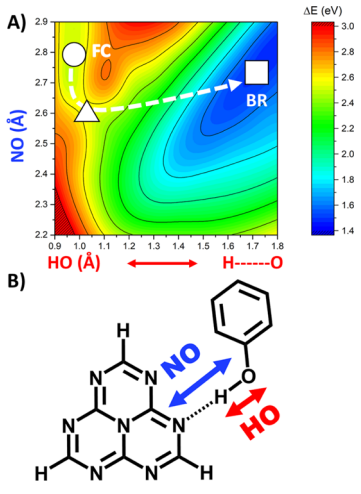

Figure 6. (A) 2D relaxed potential energy surface of the S_1 excited state of the heptazine–phenol (Hz–PhOH) complex computed at the ADC(2) level. The reaction coordinates are the OH bond length of PhOH and the distance between the O-atom of PhOH and N-atom of Hz, see (B). The circle designates the energy minimum of the LE state in the FC region. The square indicates the equilibrium geometry of the $^{\bullet}$HzH···PhO$^{\bullet}$ biradical (BR) formed by H-atom transfer. A saddle point (marked by the triangle) separates the two energy minima.

DOI: 10.1021/acs.jpcc.9b08842
J. Phys. Chem. C 2019, 123, 29580–29588

PCET reaction. The saddle point (transition state) on this 2D relaxed surface was located and used as the starting guess for a full optimization of the transition state with the ADC(2) method. Analysis of the eigenvalues of the Hessian confirmed there was only a single imaginary frequency, implying a first-order saddle point. The difference between the energy of the transition state and the energy minimum of the S_1 state in the Franck Condon (FC) zone defines the reaction barrier $\Delta E^{\ddagger}$. The reaction barriers are listed in Table 1.

Figure 6A shows the 2D relaxed S_1 potential energy surface of the Hz−PhOH complex. For small OH distances, the H-atom is covalently bonded to the oxygen atom of PhOH and forms a hydrogen bond with a peripheral nitrogen atom of Hz. For large OH distances, on the other hand, the H-atom is covalently bonded to the nitrogen atom of Hz [forming the heptazinyl ($HzH^{\bullet}$) radical] and is hydrogen-bonded with the phenoxyl ($PhO^{\bullet}$) radical. The 2D relaxed energy surface clearly exhibits two minima. The minimum for small OH distances is the energy minimum of the LE state in the FC region (indicated by the white circle in Figure 6A). The second minimum at large OH distances (indicated by the white square in Figure 6A) represents the $^{\bullet}HzH\cdots PhO^{\bullet}$ biradical (BR). For the ES-PCET transfer to occur, the photoexcited complex has to overcome the barrier separating the two minima, which is indicated by the triangle in Figure 6A. At the saddle point, the wave function of the S_1 state changes from a $\pi\pi^*$ state of LE character to a $\pi\pi^*$ state of CT character. For the Hz−PhOH complex, the energy of the saddle point is 2.68 eV above the energy minimum of the S_0 state and the barrier height is 0.167 eV.

Figure 7 shows the 2D relaxed S_1 energy surfaces of the CN−PhOH−Hz (A) and OCH_3−PhOH−Hz (B) complexes. These are the systems with the highest (CN−PhOH−Hz) and lowest (OCH_3−PhOH−Hz) barrier for the ES-PCET reaction. For CN−PhOH−Hz, the energy of the transition state is 2.89 eV above the S_0 energy minimum and the height of the barrier of the PCET reaction is 0.369 eV. The comparatively high barrier is a consequence of the electron-withdrawing character of the nitrile group of the CN−PhOH−Hz complex, which leads to a blue shift of the CT state compared to the Hz−PhOH complex (S_{CT}^{GS} = 3.86 eV, see Table S3 in the Supporting Information). The methoxy group of the OCH_3−PhOH complex (Figure 7B), on the other hand, is a relatively strong electron-donating group which causes a substantial red shift of the CT state (S_{CT}^{GS} = 2.80 eV, see Table S3 in the Supporting Information). The vertical excitation energies of the CT states of CN−PhOH−Hz and OCH_3−PhOH−Hz differ by more than 1.0 eV. For OCH_3−PhOH−Hz, the redshift of the CT state is large enough to eliminate the barrier on the S_1 potential energy surface; see Figure 7B. The theoretically predicted barrierless ES-PCET reaction is consistent with the experimental observations for OCH_3−PhOH: no observable fast PL component attributable to a hydrogen-bonded complex and no significant KIE.

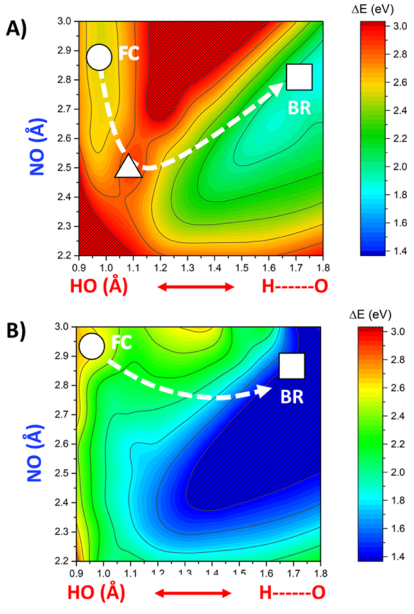

Figure 7. (A) 2D relaxed potential energy surface of the S_1 excited state of the CN−PhOH−Hz and the OCH_3−PhOH−Hz (B) complexes computed at the ADC(2) level. See caption of Figure 6 for the definition of the reaction coordinates. (B) OCH_3−PhOH−Hz complex exhibits a barrierless S_1 potential energy surface.

Additional ab initio data (vertical excitation energies of the LE and CT states and vibrational stabilization energies of the LE state) are collected in Table S3 in the Supporting Information. The molecular structures of the BRs and the transition states of the six Hz−R−PhOH complexes are displayed in Figures S24 and S25 of the Supporting Information, respectively. The lengths of the OH···N hydrogen bonds at the transition state are specified in this figure. While the vertical excitation energies of the S_1 states, S^{iGS}, and the minimum-to-minimum excitation energies of the LE states, S_1^{min}, differ by merely 0.02 eV, the energies of the transition state, S_1^{TS}, vary substantially for the substituents R on PhOH, resulting in a significant variation of the barrier height $\Delta E^{\ddagger}$. The stronger the electron-donating character of the substituent, the lower the barrier. Importantly, the barrier height $\Delta E^{\ddagger}$ and the vertical excitation energy of the CT state, S_{CT}^{GS}, are strongly correlated. While the latter decreases by about 1.0 eV from the CN substituent to the OCH_3 substituent, the barrier height changes by 0.37 eV. These findings imply that the vertical excitation energy of the CT state, which is much easier to compute than the energy of the transition state, can be used as a proxy for the relative barrier height in future ab initio screening studies of carbon nitride photocatalysts.

2.5. Implications for Molecular Design. While the limited solubility of TAHz restricts our ability to reliably estimate pK_a and ΔG_{PCET} values, we can readily infer that proton motion must play a significant role in the photochemical reactivity of TAHz because the excited state reduction potential of the free chromophore is 1.48 V versus SHE (see Section SVII). Comparing the potentials for the isolated half reactions, this reduction potential would be insufficient to drive oxidation of any of the PhOHs in the series that we have studied here. Fortunately, we can glean critical insight by examining the ab initio computational results for the barrier height $\Delta E^{\ddagger}$ of the ES-PCET reaction from PhOH to the Hz core. The computed $\Delta E^{\ddagger}$ values exhibit a reasonable correlation with the rate constants for excited state quenching plotted in Figure 8. We observe that the greater the degree of electron-donating character of the substituent on the PhOH, the lower the value of $\Delta E^{\ddagger}$ and the faster the excited state quenching. This trend suggests that chemically inverting this effect, appending strongly electron-withdrawing moieties to the heptazine core, could significantly increase the rate constant for the ES-PCET reaction of a hydrogen-bonded Hz−water

DOI: 10.1021/acs.jpcc.9b08842
J. Phys. Chem. C 2019, 123, 29580−29588

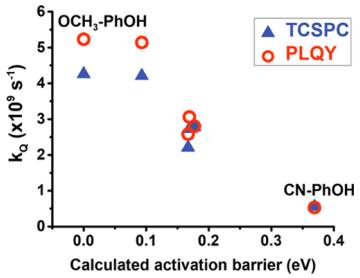

Figure 8. Correlation between the calculated activation barrier and the excited state quenching rate constants, determined by PLQY (red open circles) and TCSPC (blue triangles). Overall, we see a significant increase in the excited-state quenching rate as the phenol substituent becomes more electron-donating. We see a greater difference between the two methods as the calculated activation barrier decreases, indicating that the rate of ES-PCET is limited by diffusion and complex formation.

complex. However, it is interesting to note that for PhOH derivatives with similar oxidation potentials, Cl−PhOH, PhOH, and Br−PhOH, the effect of hydrogen bonding is evident. The PhOHs with lower pK_a's have larger K_A values, stronger hydrogen bonds, and greater quenching rate constants. Therefore, it is important to consider both electrochemical potentials and hydrogen-bonding strengths for photocatalyst design. Achieving efficient intermolecular ES-PCET in hydrogen-bonded aza−arene−water complexes could lay the groundwork to kick off a variety of future applications with the potential to utilize compelling reactions with these photogenerated hydroxyl and heptazinyl radical species, including hydrogen production, CO_2 reduction, and municipal waste-water decontamination.

3. CONCLUSIONS

We aim to control the rate of ES-PCET between heptazine chromophores and hydroxylic compounds by tuning the excited state barrier height for H-atom abstraction. We hypothesized that this tunability could be achieved by adding electron-donating groups to the hydroxylic compound (Figure 1). We present a combined experimental and theoretical study to assess the validity of such a design strategy by adding electron-donating groups to PhOH, acting as a model hydroxylic species. In support of our hypothesis, we observe increased quenching rate constants for PhOH derivatives with more electron-donating substituents. The ES-PCET reactivity is found to be governed by the barrier height $\Delta E^{\ddagger}$ on the potential energy surface of the long-lived S_1 state of the TAHz−PhOH complex, which in turn scales with the vertical excitation energy of the CT state. In the case of the most electron-donating hydroxylic compound, OCH_3−PhOH, we computationally predict and experimentally verify the excited state H-atom transfer reaction becomes barrierless in the S_1 excited state of the hydrogen-bonded complex. This increased reactivity does not come at a significant cost of hydrogen bonding as the K_A values for OCH_3−PhOH−TAHz and PhOH−TAHz are essentially the same.

It is a common practice in photocatalytic hydrogen evolution experiments to use sacrificial electron donors such as triethanolamine, triethylamine, or methanol.[5] However, systematic investigations as to how excited state dynamics influence reactivity is lacking. Herein, we presented a systematic and theory-supported analysis of the ES-PCET reactivity for the TAHz photocatalyst with substituted PhOHs as sacrificial electron donors. The oxidation potentials, E_0, of the electron donors vary from 2.03 V (CN−PhOH) to 1.68 V (OCH_3−PhOH) (Table 1). The ab initio computed reaction barriers vary from 0.369 eV for CN−PhOH to zero (no barrier) for OCH_3−PhOH, following closely the trend of the oxidation potentials. While it is comparatively easy to photo-oxidize sacrificial electron donors with low oxidation potentials, the challenge lies in the efficient photo-oxidation of water molecules with visible light. Rather than lowering the oxidation potential of the solvent, the reduction potential of the photocatalyst should be increased such that hydrogen-bonded water molecules can be oxidized in a barrierless and therefore efficient ES-PCET reaction, thus removing the need for sacrificial electron donors. We conjecture that this can be achieved with Hz-based photocatalysts by adding strong electron-withdrawing groups to the Hz core. Synthetic efforts guided by ab initio electronic structure calculations are currently underway in our laboratories to experimentally develop this scenario. Interesting questions remain regarding the nature of the proton-transfer mechanism (tunneling vs barrier crossing) and the ultimate fate of the radicals that are produced.

■ ASSOCIATED CONTENT

Supporting Information

The Supporting Information is available free of charge at https://pubs.acs.org/doi/10.1021/acs.jpcc.9b08842.

Materials and methods, K_A determination, k_Q determination, TR-PL, electrochemistry, and additional calculations can be found in the Supporting Information (PDF)

■ AUTHOR INFORMATION

Corresponding Author

*Email: schlenk@uw.edu.

ORCID

Emily J. Rabe: 0000-0002-9397-049X
Kathryn L. Corp: 0000-0002-2015-386X
Andrzej L. Sobolewski: 0000-0001-5718-489X
Wolfgang Domcke: 0000-0001-6523-1246
Cody W. Schlenker: 0000-0003-3103-402X

Author Contributions

E.J.R. and K.L.C. contributed equally. The manuscript was written through contributions of all authors. All authors have given approval to the final version of the manuscript.

Notes

The authors declare no competing financial interest.

■ ACKNOWLEDGMENTS

This work is based on research that was supported in part by the Washington Research Foundation and the University of Washington Clean Energy Institute (CEI). A portion of this work was conducted at the Molecular Analysis Facility, a National Nanotechnology Coordinated Infrastructure site at the University of Washington, which is supported in part by the National Science Foundation (grant ECC-1542101), Office of Naval Research Defense University Research Instrumentation Program (grant N00014-14-1-0757), University of Washington, Molecular Engineering & Sciences Institute, Clean Energy Institute, and National Institutes of

DOI: 10.1021/acs.jpcc.9b08842
J. Phys. Chem. C 2019, 123, 29580−29588

Health. C.W.S. acknowledges that a portion of this material is based upon work supported by the US National Science Foundation (NSF) under grant no. [1846480]. The work at the Technical University of Munich (W.D.) was supported by the Munich Centre for Advanced Photonics (MAP). A.L.S. acknowledges support by the Alexander von Humboldt Research Award.

REFERENCES

(1) Mora, S. J.; Odella, E.; Moore, G. F.; Gust, D.; Moore, T. A.; Moore, A. L. Proton-Coupled Electron Transfer in Artificial Photosynthetic Systems. *Acc. Chem. Res.* **2018**, *51*, 445−453.
(2) Wang, Q.; Wang, X.; Yu, Z.; Jiang, X.; Chen, J.; Tao, L.; Wang, M.; Shen, Y. Artificial Photosynthesis of Ethanol Using Type-II g-C3N4/ZnTe Heterojunction in Photoelectrochemical CO2 Reduction System. *Nano Energy* **2019**, *60*, 827−835.
(3) Wang, J. L.; Xu, L. J. Advanced Oxidation Processes for Wastewater Treatment: Formation of Hydroxyl Radical and Application. *Crit. Rev. Environ. Sci. Technol.* **2012**, *42*, 251−325.
(4) Li, H.; Gan, S.; Wang, H.; Han, D.; Niu, L. Intercorrelated Superhybrid of AgBr Supported on Graphitic-C3N4-Decorated Nitrogen-Doped Graphene: High Engineering Photocatalytic Activities for Water Purification and CO2 Reduction. *Adv. Mater.* **2015**, *27*, 6906−6913.
(5) Pearson, R. M.; Lim, C.-H.; McCarthy, B. G.; Musgrave, C. B.; Miyake, G. M. Organocatalyzed Atom Transfer Radical Polymerization Using N-Aryl Phenoxazines as Photoredox Catalysts. *J. Am. Chem. Soc.* **2016**, *138*, 11399−11407.
(6) Theriot, J. C.; Lim, C.-H.; Yang, H.; Ryan, M. D.; Musgrave, C. B.; Miyake, G. M. Organocatalyzed Atom Transfer Radical Polymerization Driven by Visible Light. *Science* **2016**, *352*, 1082−1086.
(7) Ong, W.-J.; Tan, L.-L.; Ng, Y. H.; Yong, S.-T.; Chai, S.-P. Graphitic Carbon Nitride (g-C3N4)-Based Photocatalysts for Artificial Photosynthesis and Environmental Remediation: Are We a Step Closer To Achieving Sustainability? *Chem. Rev.* **2016**, *116*, 7159−7329.
(8) Concepcion, J. J.; Brennaman, M. K.; Deyton, J. R.; Lebedeva, N. V.; Forbes, M. D. E.; Papanikolas, J. M.; Meyer, T. J. Excited-State Quenching by Proton-Coupled Electron Transfer. *J. Am. Chem. Soc.* **2007**, *129*, 6968−6969.
(9) Weinberg, D. R.; Gagliardi, C. J.; Hull, J. F.; Murphy, C. F.; Kent, C. A.; Westlake, B. C.; Paul, A.; Ess, D. H.; McCafferty, D. G.; Meyer, T. J. Proton-Coupled Electron Transfer. *Chem. Rev.* **2012**, *112*, 4016−4093.
(10) Lennox, J. C.; Kurtz, D. A.; Huang, T.; Dempsey, J. L. Excited-State Proton-Coupled Electron Transfer: Different Avenues for Promoting Proton/Electron Movement with Solar Photons. *ACS Energy Lett.* **2017**, *2*, 1246−1256.
(11) Damrauer, N. H.; Hodgkiss, J. M.; Rosenthal, J.; Nocera, D. G. Observation of Proton-Coupled Electron Transfer by Transient Absorption Spectroscopy in a Hydrogen-Bonded, Porphyrin Donor−Acceptor Assembly. *J. Phys. Chem. B* **2004**, *108*, 6315−6321.
(12) Eisenhart, T. T.; Dempsey, J. L. Photo-induced Proton-Coupled Electron Transfer Reactions of Acridine Orange: Comprehensive Spectral and Kinetics Analysis. *J. Am. Chem. Soc.* **2014**, *136*, 12221−12224.
(13) Liu, X.; Karsili, T. N. V.; Sobolewski, A. L.; Domcke, W. Photocatalytic Water Splitting with the Acridine Chromophore: A Computational Study. *J. Phys. Chem. B* **2015**, *119*, 10664−10672.
(14) Reimers, J. R.; Cai, Z.-L. Hydrogen Bonding and Reactivity of Water to Azines in Their S1 (n,pi*) Electronic Excited States in the Gas Phase and in Solution. *Phys. Chem. Chem. Phys.* **2012**, *14*, 8791.
(15) Whitten, D. G.; Lee, Y. J. Photochemistry of Aza Aromatics. Identification of the Reactive Intermediate in the Photoreduction of Acridine. *J. Am. Chem. Soc.* **1971**, *93*, 961−966.
(16) Peon, J.; Tan, X.; Hoerner, J. D.; Xia, C.; Luk, Y. F.; Kohler, B. Excited State Dynamics of Methyl Viologen. Ultrafast Photoreduction in Methanol and Fluorescence in Acetonitrile. *J. Phys. Chem. A* **2001**, *105*, 5768−5777.
(17) Stermitz, F. R.; Wei, C. C.; O'Donnell, C. M. Photochemistry of n-Heterocycles. V. Photochemistry of Quinoline and Some Substituted Quinoline Derivatives. *J. Am. Chem. Soc.* **1970**, *92*, 2745−2752.
(18) Arias-Rotondo, D. M.; McCusker, J. K. The Photophysics of Photoredox Catalysis: A Roadmap for Catalyst Design. *Chem. Soc. Rev.* **2016**, *45*, 5803−5820.
(19) Corp, K. L.; Schlenker, C. W. Ultrafast Spectroscopy Reveals Electron-Transfer Cascade That Improves Hydrogen Evolution with Carbon Nitride Photocatalysts. *J. Am. Chem. Soc.* **2017**, *139*, 7904−7912.
(20) Zhang, G.; Lin, L.; Li, G.; Zhang, Y.; Savateev, A.; Zafeiratos, S.; Wang, X.; Antonietti, M. Ionothermal Synthesis of Triazine−Heptazine-Based Copolymers with Apparent Quantum Yields of 60 % at 420 nm for Solar Hydrogen Production from "Sea Water". *Angew. Chem., Int. Ed.* **2018**, *57*, 9372−9376.
(21) Wang, X.; Maeda, K.; Thomas, A.; Takanabe, K.; Xin, G.; Carlsson, J. M.; Domen, K.; Antonietti, M. A Metal-Free Polymeric Photocatalyst for Hydrogen Production from Water Under Visible Light. *Nat. Mater.* **2008**, *8*, 76.
(22) Ullah, N.; Chen, S.; Zhao, Y.; Zhang, R. Photoinduced Water−Heptazine Electron-Driven Proton Transfer: Perspective for Water Splitting with g-C3N4. *J. Phys. Chem. Lett.* **2019**, *10*, 4310−4316.
(23) Domcke, W.; Ehrmaier, J.; Sobolewski, A. L. Solar Energy Harvesting with Carbon Nitrides and N-Heterocyclic Frameworks: Do We Understand the Mechanism? *ChemPhotoChem* **2019**, *3*, 10−23.
(24) Ehrmaier, J.; Karsili, T. N. V.; Sobolewski, A. L.; Domcke, W. Mechanism of Photocatalytic Water Splitting with Graphitic Carbon Nitride: Photochemistry of the Heptazine−Water Complex. *J. Phys. Chem. A* **2017**, *121*, 4754−4764.
(25) Rabe, E. J.; Corp, K. L.; Sobolewski, A. L.; Domcke, W.; Schlenker, C. W. Proton-Coupled Electron Transfer from Water to a Model Heptazine-Based Molecular Photocatalyst. *J. Phys. Chem. Lett.* **2018**, *9*, 6257−6261.
(26) Caspar, J. V.; Meyer, T. J. Photochemistry of tris(2,2'-bipyridine)ruthenium(2+) ion (Ru(bpy)32+) Solvent effects. *J. Am. Chem. Soc.* **1983**, *105*, 5583−5590.
(27) McCusker, J. K. Electronic Structure in the Transition Metal Block and Its Implications for Light Harvesting. *Science* **2019**, *363*, 484−488.
(28) Turro, N. J.; Ramamurthy, V.; Scaiano, J. C. *Principles of Molecular Photochemistry: An Introduction*; University Science Books: Sausalito, California, 2009.
(29) Ehrmaier, J.; Rabe, E. J.; Pristash, S. R.; Corp, K. L.; Schlenker, C. W.; Sobolewski, A. L.; Domcke, W. Singlet−Triplet Inversion in Heptazine and in Polymeric Carbon Nitrides. *J. Phys. Chem. A* **2019**, *123*, 8099−8108.
(30) Barman, N.; Singha, D.; Sahu, K. Fluorescence Quenching of Hydrogen-Bonded Coumarin 102-Phenol Complex: Effect of Excited-State Hydrogen Bonding Strength. *J. Phys. Chem. A* **2013**, *117*, 3945−3953.
(31) Hossen, T.; Sahu, K. New Insights on Hydrogen-Bond-Induced Fluorescence Quenching Mechanism of C102−Phenol Complex via Proton Coupled Electron Transfer. *J. Phys. Chem. A* **2018**, *122*, 2394−2400.
(32) Bronner, C.; Wenger, O. S. Proton-Coupled Electron Transfer between 4-Cyanophenol and Photoexcited Rhenium(I) Complexes with Different Protonatable Sites. *Inorg. Chem.* **2012**, *51*, 8275−8283.
(33) Bronner, C.; Wenger, O. S. Kinetic Isotope Effects in Reductive Excited-State Quenching of Ru(2,2′-bipyrazine)32+ by Phenols. *J. Phys. Chem. Lett.* **2012**, *3*, 70−74.
(34) Warren, J. J.; Tronic, T. A.; Mayer, J. M. Thermochemistry of Proton-Coupled Electron Transfer Reagents and its Implications. *Chem. Rev.* **2010**, *110*, 6961−7001.
(35) Dongare, P.; Bonn, A. G.; Maji, S.; Hammarström, L. Analysis of Hydrogen-Bonding Effects on Excited-State Proton-Coupled

DOI: 10.1021/acs.jpcc.9b08842
J. Phys. Chem. C 2019, 123, 29580−29588

Electron Transfer from a Series of Phenols to a Re(I) Polypyridyl Complex. *J. Phys. Chem. C* **2017**, *121*, 12569−12576.
(36) Petersson, J.; Hammarström, L. Ultrafast Electron Transfer Dynamics in a Series of Porphyrin/Viologen Complexes: Involvement of Electronically Excited Radical Pair Products. *J. Phys. Chem. B* **2015**, *119*, 7531−7540.
(37) Hossen, T.; Sahu, K. Photo-induced Electron Transfer or Proton-Coupled Electron Transfer in Methylbipyridine/Phenol Complexes: A Time-Dependent Density Functional Theory Investigation. *J. Phys. Chem. A* **2019**, *123*, 8122−8129.
(38) Guerard, J. J.; Arey, J. S. Critical Evaluation of Implicit Solvent Models for Predicting Aqueous Oxidation Potentials of Neutral Organic Compounds. *J. Chem. Theory Comput.* **2013**, *9*, 5046−5058.
(39) Yamaji, M.; Oshima, J.; Hidaka, M. Verification of the Electron/Proton Coupled Mechanism for Phenolic H-atom Transfer Using a Triplet π,π^* Carbonyl. *Chem. Phys. Lett.* **2009**, *475*, 235−239.
(40) Snellenburg, J. J.; Laptenok, S. P.; Seger, R.; Mullen, K. M.; van Stokkum, I. H. M. Glotaran: A Java-Based Graphical User Interface for the R Package TIMP. *J. Stat. Softw.* **2012**, *49*, 1−22.
(41) Schirmer, J. Beyond the Random-Phase Approximation: A New Approximation Scheme for the Polarization Propagator. *Phys. Rev. A: At., Mol., Opt. Phys.* **1982**, *26*, 2395−2416.

DOI: 10.1021/acs.jpcc.9b08842
J. Phys. Chem. C 2019, 123, 29580−29588